Available online at www.sciencedirect.com
SCIENCE DIRECT®
Journal of Sound and Vibration 292 (2006) 552–570
JOURNAL OF SOUND AND VIBRATION
www.elsevier.com/locate/jsvi

A comparison of time delay estimators for the detection of leak noise signals in plastic water distribution pipes

Y. Gao*, M.J. Brennan, P.F. Joseph

Institute of Sound and Vibration Research, University of Southampton, Southampton SO17 1BJ, UK

Received 8 July 2004; received in revised form 5 August 2005; accepted 9 August 2005
Available online 3 November 2005

Abstract

The position of a leak in buried water distribution pipes, may be determined by accurate estimation of the time delay between two measured acoustic signals. By using a model for the wave propagation along plastic pipes, various time delay estimators using cross-correlation are compared in this paper for their ability to locate a leak in plastic pipes. The estimators of interest are the ROTH impulse response, the smoothed coherence transform (SCOT), the WIENER, the phase transform (PHAT) and the maximum likelihood (ML) estimators. For leak detection in buried plastic water pipes it is found that the SCOT estimator is particularly suited to this purpose. The accuracy of the estimators is also discussed. It is found that random errors introduced by random noise on the signal measurements are insignificant compared with the resolution of the time delay estimators imposed by the low-pass filtering characteristics of the pipe. Limited experimental results are presented to support the findings.

1. Introduction

A leak from a water supply pipe system generates noise, which can be used for leak detection and location. The correlation technique [1–3], which is used to estimate the time delay between two measured acoustic/vibration signals, is central to this process. Important factors in the detectability of the leak are the signal-to-noise ratio (SNR) and the amount of a priori knowledge, principally, the sound propagation wavespeed c in the pipe. A sensor is placed either side of the leak, and the distance between the two sensors is usually measured on-site or read off system maps, whereas the propagation wavespeed is normally estimated using pipe data [4,5] or measured on-site using a simulated leak [6].

Various time delay estimation techniques have been proposed and implemented over the years. Some of the most important are summarised in Refs. [7–9]. These techniques are based on the cross-correlation of two measured signals and include the basic cross-correlation (BCC) and generalised cross-correlation (GCC) methods, of which the BCC method is a trivial example. The essential difference between the BCC and the GCC methods, is that with the latter, the signals are passed though filters (pre-filtering) prior to performing the cross-correlation. The advantages of pre-filtering are two-fold: (i) to enhance the signals in the frequency

*Corresponding author. Tel.: +44 23 8059 3756; fax: +44 23 8059 3190.
E-mail address: gy@isvr.soton.ac.uk (Y. Gao).

0022-460X/$ - see front matter © 2005 Elsevier Ltd. All rights reserved.
doi:10.1016/j.jsv.2005.08.014

Nomenclature

$\tau, \tau_{peak}, \hat{\tau}_{peak}$ lag of time; time delay at the peak value and its estimate
$x_1(t), x_2(t)$ acoustic/vibration signals
$n_1(t), n_2(t)$ background noise
$X_1(f), X_2(f)$ Fourier transforms of $x_1(t)$ and $x_2(t)$, respectively
d distance between two sensor signals
d_1, d_2 relative distance between the leak and signals $x_1(t)$ and $x_2(t)$
c propagation wavespeed
$R_{x_1x_2}(\tau), \hat{R}_{x_1x_2}(\tau)$ cross-correlation function between signals $x_1(t)$ and $x_2(t)$ and its estimate
$R^g_{x_1x_2}(\tau), \hat{R}^g_{x_1x_2}(\tau)$ GCC function between signals $x_1(t)$ and $x_2(t)$ and its estimator
$R^P_{x_1x_2}(\tau), R^R_{x_1x_2}(\tau), R^W_{x_1x_2}(\tau), R^S_{x_1x_2}(\tau), R^M_{x_1x_2}(\tau)$ the PHAT, ROTH, WIENER, SCOT, ML estimators
$R_{s_1s_2}(\tau)$ cross-correlation function between signals $s_1(t)$ and $s_2(t)$
$S_{x_1x_2}(\omega), \hat{S}_{x_1x_2}(\omega)$ CSD between signals $x_1(t)$ and $x_2(t)$ and its estimate
$\Psi_{2n}(\omega)$ frequency characteristics due to propagation effects along the pipe, which is a function of wave attenuation and the type of sensor
$S_{s_1s_2}(\omega)$ CSD between signals $s_1(t)$ and $s_2(t)$
$S_{ll}(\omega), S_{n_1n_1}(\omega), S_{n_2n_2}(\omega)$ ASD of the leak signal $l(t)$, and noise signals $n_1(t)$ and $n_2(t)$
$\Phi_{x_1x_2}(\omega)$ phase spectrum between signals $x_1(t)$ and $x_2(t)$
$\gamma^2_{x_1x_2}(\omega)$ ordinary coherence function between $x_1(t)$ and $x_2(t)$
$\Psi_g(\omega)$ frequency weighting function of the GCC function
$\Psi_P(\omega), \Psi_R(\omega), \Psi_W(\omega), \Psi_S(\omega), \Psi_M(\omega)$ frequency weighting functions of the PHAT, ROTH, WIENER, SCOT, ML estimators
$H(\omega, x)$ frequency response function between the signal measured at the sensor location and the pressure at the leak location
$\delta(\tau)$ Dirac delta function
$\sigma^2_{\hat{\tau}_{peak}}, \sigma_{\hat{\tau}_{peak}}$ variance and standard derivation of $\hat{\tau}_{peak}$
σ_z standard deviation of the first derivative of the cross-correlation function
$\left\lvert\frac{\partial E[z]}{\partial \tau}\right\rvert_{\tau=\tau_{peak}}$ slope of the cross-correlation function at $\tau = \tau_{peak}$
$G(\omega)$ band-pass filter
$\Delta\omega, \omega_0, \omega_1$ frequency bandwidth of band-pass filter; lower and upper cut-off frequencies of band-pass filter
ω_c centre frequency of a band-pass filter
$\Delta\tau$ temporal bandwidth, i.e., resolution of the time delay estimator

bands where the SNR is high, thereby suppressing the signals outside these bands, and (ii) to pre-whiten the signals in order to sharpen the peak in the cross-correlation function. Knapp and Carter discussed the characteristics of five GCC methods and compared them with the BCC method [7]. In this paper, we compare the same GCC methods with the BCC method for the purpose of leak detection in buried plastic water pipes to determine which method is best suited to this particular application.

The five GCC methods considered are the ROTH impulse response (proposed by Peter Roth), the smoothed coherence transform (SCOT), the WIENER (after its inventor Norbert Wiener), the phase transform (PHAT) and the maximum likelihood (ML) estimators.

In the ROTH estimator [10], rather than determining the cross-correlation between two signals, the signals are used to deduce the impulse response of the system. This is achieved by normalising the cross-spectrum by the auto-spectrum of one of the signals (the input), prior to transforming back to the time domain. The rationale for this procedure is that it removes the effects of the input, thus deducing the system delay more accurately. However, because the input (leak) spectrum cannot be measured directly it is difficult to see how this method could be beneficial for leak detection, but it is included in this paper for completeness.

The SCOT estimator favours neither sensor signal and was developed by Carter et al. [11] to suppress the undesirable effects of strong tonal signals in weak broad-band signals. In the SCOT estimator the cross-spectrum is normalised by the square-root of the product of the auto-spectra of the two signals. For leak detection in pipes we show this to be a worthwhile procedure; the reasons why this is so, and an alternative interpretation of this processor, is given in Section 3.

To sharpen the peak in the cross-correlation function, the PHAT estimator has been proposed [12]. In this estimator the modulus of the cross-spectrum is 'flattened' prior to transformation to the time domain. Thus, only phase information is used for performing the time delay estimation. The deficiency in this technique is that it does not take into account the coherence between the two signals and thus gives equal weight to all frequencies regardless of signal strength.

Another important estimator for time delay is the ML estimator. Hannan and Thomson derived this for band limited random signals corrupted by white noise [13]. This estimator weights the cross-spectrum according to the SNR, giving most weight to the phase spectrum that leads to the minimum variance of the time delay estimate.

The WIENER estimator [14] involves the multiplication of the cross-spectrum by the coherence between the two signals prior to transformation to the time domain. It is suggested in Ref. [14] that this estimator is preferable to the ML estimator in certain situations, as the ML estimator has the effect of overemphasizing as well as underemphasizing the signals at certain frequencies.

In this paper, the analytical model of wave propagation along a fluid-filled pipe derived previously by the authors [15], is used to compare performance of the time delay estimators. To study their accuracy, the expression for the uncertainty in the time delay estimates are derived and compared. They are further compared with the resolution of the time delay estimates introduced by the low-pass filtering properties of the pipe. The analysis uses the general expression for the variance of a time delay estimate derived by Carter [16]. To assist the reader, and because the analysis is not widely available in the literature, the derivation of this expression is given in Appendix A. To support the theoretical analysis, the time delay estimators are used to predict the location of a leak using experimental data obtained from a buried PVC water pipe. Their performance in relation to this experimental data is compared and discussed. Notations are explained in nomenclature.

2. Leak detection using the basic cross-correlation method

To perform leak detection, vibration or acoustic signals are measured at two access points using sensors such as accelerometers or hydrophones, either side of the location of a suspected leak, as shown in Fig. 1. If a leak exists, a distinct peak may be found in the cross-correlation of the two signals $x_1(t)$ and $x_2(t)$. This gives the time delay τ_{peak} that corresponds to the difference in arrival times between the acoustic signals at each sensor. The location of the leak relative to one of the measurement points, d_1, can be calculated using the relationship between the time delay τ_{peak}, the distance d between the access points, and the propagation wavespeed c in the buried pipe,

$$d_1 = \frac{d - c\tau_{peak}}{2}. \tag{1}$$

If $x_1(t)$ and $x_2(t)$ are two stationary random signals with zero mean, the cross-correlation function is defined by [17]

$$R_{x_1x_2}(\tau) = E[x_1(t)x_2(t+\tau)], \tag{2}$$

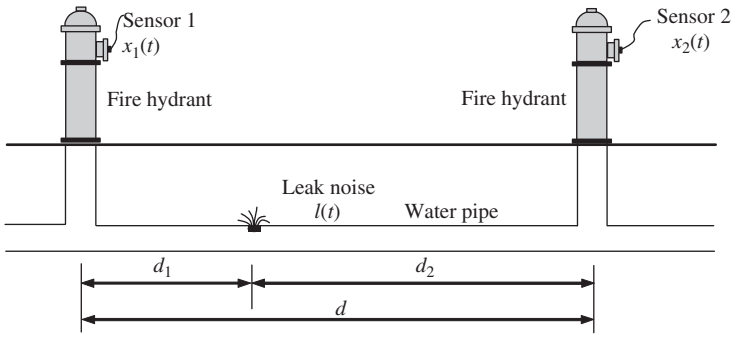

Fig. 1. Schematic of a pipe with a leak bracketed by two sensors.

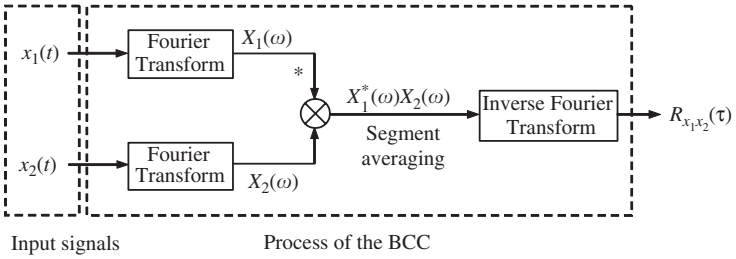

Fig. 2. Schematic of the implementation of the BCC function.

where τ is the time lag and $E[\bullet]$ is the expectation operator. The value of τ that maximises Eq. (2) provides an estimate τ_{peak} of the time delay. A procedure to calculate the BCC function using sampled data is illustrated in Fig. 2. The BCC estimator can be obtained from the inverse Fourier transform of $X_1^*(f)X_2(f)$ and scaled appropriately for normalisation, where $X_1(f)$ and $X_2(f)$ are the Fourier transforms of $x_1(t)$ and $x_2(t)$, respectively, and * denotes complex conjugation. The cross-correlation function, $R_{x_1x_2}(\tau)$, is related to the cross-spectral density (CSD), $S_{x_1x_2}(\omega)$, by the inverse Fourier transform [17]

$$R_{x_1x_2}(\tau) = F^{-1}\{S_{x_1x_2}(\omega)\} = \frac{1}{2\pi}\int_{-\infty}^{+\infty} S_{x_1x_2}(\omega)e^{i\omega\tau}\,d\omega, \tag{3}$$

where $F^{-1}\{\}$ denotes the inverse Fourier transform. In practice, only an estimate of the CSD can be obtained since it is derived from finite time observations of $x_1(t)$ and $x_2(t)$. However, to simplify the derivation of various time delay estimators, the ideal CSD is used in this paper.

Assuming that the signals are generated from a leak and measured using two separate acoustic sensors in the presence of background noise, the measured signals can be represented by

$$x_1(t) = s_1(t) + n_1(t), \tag{4}$$

and

$$x_2(t) = s_2(t) + n_2(t), \tag{5}$$

where $s_1(t)$, $s_2(t)$, $n_1(t)$ and $n_2(t)$ are assumed to be stationary random processes. If the noise at each sensor is assumed to be uncorrelated with each other and with the signals, the cross-correlation function between signals $x_1(t)$ and $x_2(t)$ is given by

$$R_{x_1x_2}(\tau) = R_{s_1s_2}(\tau). \tag{6}$$

The CSD $S_{x_1x_2}(\omega)$ between two signals $x_1(t)$ and $x_2(t)$ measured at positions $x = d_1$ and $x = d_2$, is given by

$$S_{x_1x_2}(\omega) = \frac{1}{2\pi}\lim_{T\to\infty} E\left[\frac{X_{1T}^*(\omega)X_{2T}(\omega)}{T}\right] = H^*(\omega, d_1)H(\omega, d_2)S_{ll}(\omega), \tag{7}$$

where $S_{ll}(\omega)$ is the auto-spectral density (ASD) of the acoustic pressure generated by the leak signal $l(t)$ measured at the leak location, and $H(\omega, x)$ is the frequency response function between the signal measured by the sensor and the pressure at the leak location at a distance x, and for an infinite pipe is given by [18]

$$H(\omega, x) = (i\omega)^n A_n e^{-i\omega x/c}e^{-\omega\beta x}, \tag{8}$$

where β is a measure of the loss within the pipe wall [15], and A_n is related to the pipe wall properties and the type of sensor used. The subscript n takes the values of $n = 0$, 1 and 2, corresponding to measurements of either pressure, radial velocity or radial acceleration of the pipe wall, respectively. Combining Eqs. (7) and (8), the CSD can be written as

$$S_{x_1x_2}(\omega) = A_n^2\Psi_{2n}(\omega)e^{i\omega T_0}S_{ll}(\omega), \tag{9}$$

where $\Psi_{2n}(\omega) = \omega^{2n}e^{-\omega\beta d}$ and $T_0 = -(d_2 - d_1)/c$. Since multiplication in one domain corresponds to convolution in the transformed domain, the BCC function between signals $x_1(t)$ and $x_2(t)$ in terms of the time

delay T_0, can be written as

$$R_{x_1x_2}(\tau) = A_n^2 R_{ll}(\tau) \otimes \psi_{2n}(\tau) \otimes \delta(\tau + T_0), \tag{10}$$

where $\otimes$ denotes convolution, $R_{ll}(\tau) = F^{-1}\{S_{ll}(\omega)\}$ is the auto-correlation of the leak signal, $\psi_{2n}(\tau) = F^{-1}\{\Psi_{2n}(\omega)\}$, and $\delta(\tau)$ is the Dirac delta function. An interpretation of Eq. (10) is that it represents a delta function delayed by T_0, which is broadened by the spectral characteristics of both the leak signal and the propagation from the leak location to the sensor location. Because $\psi_{2n}(\tau)$ in Eq. (10) is a function of the choice of acoustic/vibration sensors as well as the pipe, the choice of sensor will also affect the sharpness of the peak in the correlation function as well as pre-filtering operations. This is discussed in Ref. [18].

3. Leak detection using generalised cross-correlaiton methods

To accentuate the peak in the cross-correlation function associated with the time delay, the input signals can be pre-filtered. The time and frequency domain representations of this operation are depicted in Figs. 3(a) and (b), respectively. In the time domain, the signals are filtered prior to delay, multiplication, and integration, while in the frequency domain, a window or weighting function is applied to the CSD function [7] prior to performing the inverse Fourier transform. Thus the GCC function $R^g_{x_1x_2}(\tau)$ between sensor signals $x_1(t)$ and $x_2(t)$ is given by

$$R^g_{x_1x_2}(\tau) = F^{-1}\{\Psi_g(\omega)S_{x_1x_2}(\omega)\} = \frac{1}{2\pi}\int_{-\infty}^{+\infty} \Psi_g(\omega)S_{x_1x_2}(\omega)e^{i\omega\tau}\,d\omega, \tag{11}$$

where $\Psi_g(\omega)$ is a frequency weighting function. When $\Psi_g(\omega) = 1$, the GCC function reduces to the BCC function defined by Eq. (3).

The frequency weighting functions for the GCC methods discussed in this paper are listed in Table 1. These weighting functions are taken from Ref. [9], but are written in a different form to aid interpretation. It can be seen that all the weighting functions are real and thus have no effect on the phase spectrum, and hence on the time delay estimate. These time delay estimators applied to the leak detection problem illustrated in Fig. 1 are discussed below.

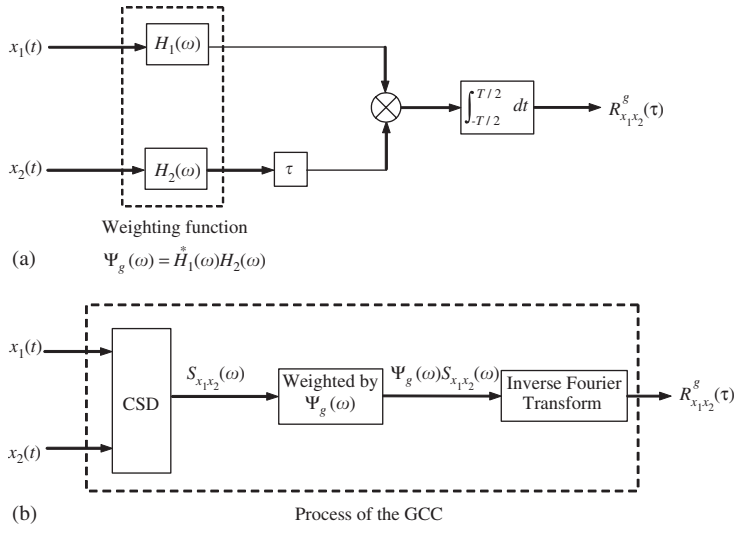

Fig. 3. Schematic of the implementation of the GCC function. (a) Time domain; and (b) frequency domain.

Table 1
Various cross-correlation methods [9]

	BCC	PHAT	WIENER	SCOT	ML	ROTH
$\Psi_g(\omega)$	1	$\frac{1}{\lvert S_{x_1x_2}(\omega)\rvert}$	$\gamma^2_{x_1x_2}(\omega)$	$\frac{\gamma_{x_1x_2}(\omega)}{\lvert S_{x_1x_2}(\omega)\rvert}$	$\frac{\gamma^2_{x_1x_2}(\omega)}{[1-\gamma^2_{x_1x_2}(\omega)]}\frac{1}{\lvert S_{x_1x_2}(\omega)\rvert}$	$\frac{1}{S_{x_1x_1}(\omega)}$

Note: $\gamma^2_{x_1x_2}(\omega)$ is the ordinary coherence function between $x_1(t)$ and $x_2(t)$, which is given by $\gamma^2_{x_1x_2}(\omega)=\frac{\lvert S_{x_1x_2}(\omega)\rvert^2}{S_{x_1x_1}(\omega)S_{x_2x_2}(\omega)}$.

3.1. The PHAT estimator

Substituting the frequency weighting function $\Psi_P(\omega)=1/|S_{x_1x_2}(\omega)|$ and the CSD $S_{x_1x_2}(\omega)$ defined by Eq. (9) into Eq. (11) gives

$$R^P_{x_1x_2}(\tau)=F^{-1}\{\Psi_P(\omega)S_{x_1x_2}(\omega)\}=\delta(\tau+T_0). \tag{12}$$

It can be seen that, by pre-whitening the measured CSD, the PHAT estimator effectively removes the effects of propagation along the pipe and the frequency characteristics of the sensors, and also the effects of the leak spectrum. For non-dispersive wave propagation, which is the case in buried plastic pipes [15,18], the result is a perfect delta function located at the time delay T_0. One disadvantage of the PHAT estimator is that it takes no account of the noise in the signals, and thus by pre-whitening, the effects of noise may be enhanced, thereby corrupting the estimate of the time delay.

3.2. The WIENER estimator

From Eqs. (4) and (5), the ASDs of signals $x_1(t)$ and $x_2(t)$, are given by

$$S_{x_1x_1}(\omega)=|H(\omega,d_1)|^2S_{ll}(\omega)+S_{n_1n_1}(\omega) \tag{13}$$

and

$$S_{x_2x_2}(\omega)=|H(\omega,d_2)|^2S_{ll}(\omega)+S_{n_2n_2}(\omega). \tag{14}$$

The weighting function for the WIENER processor $\Psi_W(\omega)$ is defined by

$$\Psi_W(\omega)=\gamma^2_{x_1x_2}(\omega)=\frac{|S_{x_1x_2}(\omega)|^2}{S_{x_1x_1}(\omega)S_{x_2x_2}(\omega)}. \tag{15}$$

This indicates that the WIENER estimator adjusts the CSD according to the value of the coherence. This method, therefore, has the desirable effect of suppressing those frequency regions where the coherence is poor. However, the pre-filtering operation does not improve the resolution of the time delay estimate as it has no effect on the sharpness of the peak in the cross-correlation function. Eqs. (13)–(15) can be substituted into Eq. (11) to give

$$R^W_{x_1x_2}(\tau)=F^{-1}\{\Psi_W(\omega)S_{x_1x_2}(\omega)\}=A_n^2R_{ll}(\tau)\otimes\psi_{2n}(\tau)\otimes h_W(\tau)\otimes\delta(\tau+T_0), \tag{16}$$

where

$$h_W(\tau)=F^{-1}\left\{\left[1+\frac{1}{|H(\omega,d_1)|^2}\frac{S_{n_1n_1}(\omega)}{S_{ll}(\omega)}\right]\left[1+\frac{1}{|H(\omega,d_2)|^2}\frac{S_{n_2n_2}(\omega)}{S_{ll}(\omega)}\right]\right\}^{-1}.$$

When the effect of background noise is negligible, i.e., $\gamma^2_{x_1x_2}(\omega)\to 1$, $R^W_{x_1x_2}(\tau)\to R_{x_1x_2}(\tau)$. In this case, the WIENER estimator is equivalent to the BCC estimator. Like the BCC estimator, the delta function in the cross-correlation function will also be smeared by the finite bandwidth of the leak spectrum, the pipe dynamics and the choice of acoustic/vibration sensors.

3.3. The SCOT estimator

The frequency weighting function for the SCOT estimator $\Psi_S(\omega)$ is given by

$$\Psi_S(\omega) = \frac{\gamma_{x_1x_2}(\omega)}{|S_{x_1x_2}(\omega)|}. \tag{17}$$

The SCOT estimator can be interpreted as a two-stage filtering process: pre-whitening represented by the denominator of $\Psi_S(\omega)$, and attenuation in the frequency regions where noise is present, by the numerator $\gamma_{x_1x_2}(\omega)$, respectively. Substituting the weighting function given by Eq. (17) into Eq. (11) gives the SCOT estimator,

$$R^S_{x_1x_2}(\tau) = F^{-1}\{\Psi_S(\omega)S_{x_1x_2}(\omega)\} = h_S(\tau) \otimes \delta(\tau + T_0), \tag{18}$$

where

$$h_S(\tau) = F^{-1}\left\{\left[1 + \frac{1}{|H(\omega,d_1)|^2}\frac{S_{n_1n_1}(\omega)}{S_{ll}(\omega)}\right]\left[1 + \frac{1}{|H(\omega,d_2)|^2}\frac{S_{n_2n_2}(\omega)}{S_{ll}(\omega)}\right]\right\}^{-1/2}.$$

It can be seen that in the noise-free case, i.e., $\gamma_{x_1x_2}(\omega) = 1$, the SCOT estimator is identical to the PHAT estimator.

3.4. The ML estimator

The frequency weighting of the ML estimator leads to the minimum variance of the time delay estimate if the signals are random Gaussian [9], which is given by

$$\Psi_M(\omega) = \frac{\gamma^2_{x_1x_2}(\omega)}{1 - \gamma^2_{x_1x_2}(\omega)}\frac{1}{|S_{x_1x_2}(\omega)|}. \tag{19}$$

In a similar way to the SCOT estimator, two pre-filtering operations are involved in the ML estimator. The pre-whitening process is represented by the second term in Eq. (19), and the first term weights the CSD according to the variance of the phase estimate. It attaches most weight when the variance of the estimated phase error is least [7]. Following the same procedures as before, the correlation estimator $R^M_{x_1x_2}(\tau)$ is given by

$$R^M_{x_1x_2}(\tau) = F^{-1}\{\Psi_M(\omega)S_{x_1x_2}(\omega)\} = h_M(\tau) \otimes \delta(\tau + T_0), \tag{20}$$

where

$$h_M(\tau) = F^{-1}\left\{\left[1 + \frac{1}{|H(\omega,d_1)|^2}\frac{S_{n_1n_1}(\omega)}{S_{ll}(\omega)}\right]\left[1 + \frac{1}{|H(\omega,d_2)|^2}\frac{S_{n_2n_2}(\omega)}{S_{ll}(\omega)}\right] - 1\right\}^{-1}.$$

3.5. The ROTH estimator

Substituting Eq. (13) and the weighting function $\Psi_R(\omega) = 1/S_{x_1x_1}(\omega)$ into Eq. (11), the ROTH estimator $R^R_{x_1x_2}(\tau)$ is given by

$$R^R_{x_1x_2}(\tau) = F^{-1}\{\Psi_R(\omega)S_{x_1x_2}(\omega)\} = A_n^2 h_R(\tau) \otimes \psi_{2n}(\tau) \otimes \delta(\tau + T_0), \tag{21}$$

where

$$h_R(\tau) = F^{-1}\{|H(\omega,d_1)|^2 + S_{n_1n_1}(\omega)/S_{ll}(\omega)\}^{-1}.$$

As can be seen in Eq. (21), the ROTH estimator is not particularly useful for leak detection in pipes due to the presence of the term $\psi_{2n}(\tau)$, which introduces smearing of the peak due to the effects of propagation along the pipe, sensor frequency characteristics, and the SNR at sensor 1.

By comparing the various GCC methods, it can be seen that the PHAT, SCOT and ML estimators involve pre-whitening of the leak signals, which sharpens the peak in the cross-correlation function. These are therefore of particular interest in this paper.

4. Variance of the time delay estimate

In this section, the variances of the time delay estimates discussed in Section 3 for the purpose of leak detection are compared. The general expression for the variance of the time delay estimate is derived in Appendix A and is given by

$$\sigma^2_{\hat{\tau}_{\text{peak}}} = \frac{2\pi}{T} \frac{\int_{-\infty}^{\infty} \omega^2 |\Psi_g(\omega)|^2 S_{x_1x_1}(\omega) S_{x_2x_2}(\omega)[1-\gamma^2_{x_1x_2}(\omega)]\,\mathrm{d}\omega}{\left[\int_{-\infty}^{\infty} \omega^2 \Psi_g(\omega)|S_{x_1x_2}(\omega)|\,\mathrm{d}\omega\right]^2}. \tag{22}$$

The variances of the specific time delay estimators given in Table 1, can be determined by substituting into Eq. (22) the various weighting functions $\Psi_g(\omega)$. To allow simple analysis, it is assumed that the coherence between the two signals $\gamma^2_{x_1x_2}(\omega)$ is constant in a frequency band $\Delta\omega = \omega_1 - \omega_0$ and is zero elsewhere, i.e.,

$$\gamma^2_{x_1x_2}(\omega) = \begin{cases} \gamma^2, & \omega_0 \leqslant |\omega| < \omega_1, \\ 0, & \text{otherwise.} \end{cases} \tag{23}$$

A similar assumption has been made by Carter [16] to discuss the effect of coherence on the ML estimator. Assuming that the coherence has the form given in Eq. (23), the variances are found to be as follows.

For the BCC and WIENER estimators,

$$\sigma^2_{\hat{\tau}_{\text{peak}}} = \frac{\pi}{T} \frac{1-\gamma^2}{\gamma^2} \frac{\int_{\omega_0}^{\omega_1} \omega^2 |S_{x_1x_2}(\omega)|^2\,\mathrm{d}\omega}{\left[\int_{\omega_0}^{\omega_1} \omega^2 |S_{x_1x_2}(\omega)|\,\mathrm{d}\omega\right]^2}. \tag{24}$$

For the PHAT, SCOT and ML estimators,

$$\sigma^2_{\hat{\tau}_{\text{peak}}} = \frac{2\pi}{T} \frac{1-\gamma^2}{\gamma^2} \frac{1}{2\int_{\omega_0}^{\omega_1} \omega^2\,\mathrm{d}\omega} = \frac{3\pi}{T} \frac{1-\gamma^2}{\gamma^2} \frac{1}{[(\omega_0+\Delta\omega)^3 - \omega_0^3]}. \tag{25}$$

For the ROTH estimator,

$$\sigma^2_{\hat{\tau}_{\text{peak}}} = \frac{\pi}{T} \frac{1-\gamma^2}{\gamma^2} \frac{\int_{\omega_0}^{\omega_1} \omega^2 \frac{S_{x_2x_2}(\omega)}{S_{x_1x_1}(\omega)}\,\mathrm{d}\omega}{\left\{\int_{\omega_0}^{\omega_1} \omega^2 \left[\frac{S_{x_2x_2}(\omega)}{S_{x_1x_1}(\omega)}\right]^{1/2} \mathrm{d}\omega\right\}^2}. \tag{26}$$

It can be seen from Eq. (25) that the variance of the PHAT, SCOT and ML estimators is governed by three factors, namely, the observation time T, the coherence γ^2, and the frequencies ω_0 and ω_1. For the other estimators, the variance is also related to the ASDs of the two signals and the CSD between them, as shown in Eqs. (24) and (26).

If we assume that the leak spectrum is 'flat', i.e., $S_{ll}(\omega) = S_0$ in the frequency range ω_0 to ω_1, the variances of the BCC and WIENER estimators can be determined by substituting Eqs. (7) and (8) into Eq. (24) to give

$$\sigma^2_{\hat{\tau}_{\text{peak}}} = \frac{\pi}{T} \frac{1-\gamma^2}{\gamma^2} \frac{\int_{\omega_0}^{\omega_1} \omega^2 \Psi^2_{2n}(\omega)\,\mathrm{d}\omega}{\left(\int_{\omega_0}^{\omega_1} \omega^2 \Psi_{2n}(\omega)\,\mathrm{d}\omega\right)^2}. \tag{27}$$

Eq. (27) shows that the variance of the BCC and WIENER estimators is governed by both the pipe properties and the choice of acoustic/vibration sensors, as $\Psi_{2n}(\omega)$ is a function of the wave attenuation and the type of sensor used. The variance of the ROTH estimator, as given by Eq. (26), is largely influenced by the background noise.

It should be noted that the variance of the time delay estimate increases as the filter bandwidth $\Delta\omega$ decreases. Consequently, it is desirable to use a filter that has a bandwidth that is as wide as possible. In

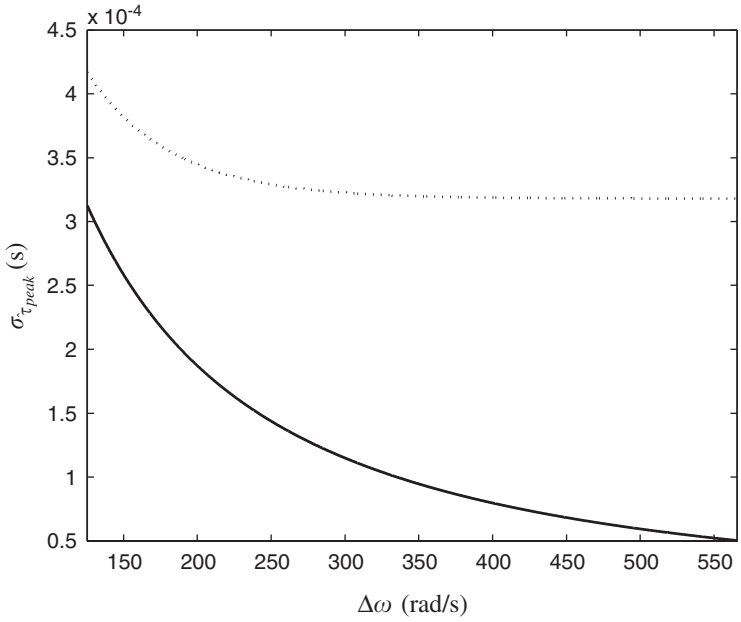

Fig. 4. The standard deviation $\sigma_{\hat{\tau}_{\text{peak}}}$ against frequency bandwidth $\Delta\omega$. PHAT, SCOT and ML estimators (——); BCC and WIENER estimators (·····) of pressure signals.

reality; however, the pipe characteristics and the distances from the sensors to the leak, govern the highest frequency of the measurable leak noise and hence ω_1. Thus to reduce the variance the only realistic options are to increase T and/or improve the coherence by using transducers with higher sensitivity.

For a typical plastic pipe with $\beta d = 0.023$ s, and assuming that $\gamma^2 = 0.2$, $T = 60$ s, and $\omega_0 = 62.8$ rad/s, the standard deviation $\sigma_{\hat{\tau}_{\text{peak}}}$ for various cross-correlation estimators is illustrated in Fig. 4. It can be seen that the standard deviation of all the estimators decreases with increasing bandwidth. Note also that the three pre-whitening estimators have the smallest variance.

5. Effect of band-pass filtering

Reliable leak detection can only be accomplished when a distinct peak can be identified in the cross-correlation function. As discussed in Section 3, the PHAT, SCOT and ML estimators pre-whiten the CSD in order to sharpen the peak in the cross-correlation function and are therefore of particular interest in this paper. In practical situations, the measured leak signals are dominated by the background noise at low frequencies and attenuated at high frequencies [15], filtering operations must be performed on the sensor signals before conducting the time domain cross-correlation. The effect of band-pass filtering of the signals on cross-correlation estimators is discussed in this section.

For non-dispersive wave propagation, the magnitude and phase of the ideal pre-whitened CSD (without considering the weighting of the coherence) between two sensor signals for time delay estimation is illustrated in Figs. 5(a) and (b), respectively. In this ideal case, a delta function in the cross-correlation is produced. In practice, the signals are band-limited, a typical phase spectrum of which is shown in Fig. 5(d). When the PHAT estimator is used on this data, the modulus is whitened as shown in Fig. 5(c), which results in a spurious peak in the correlation function at zero time lag, due to the background noise outside the frequency bandwidth of interest. It is possible that the peak in the cross-correlation function due to the time delay may be masked by the oscillatory behaviour of the spurious peak. In order to remove the possibility of these peaks, it is necessary to pass the signals through a band-pass filter prior to using the PHAT estimator.

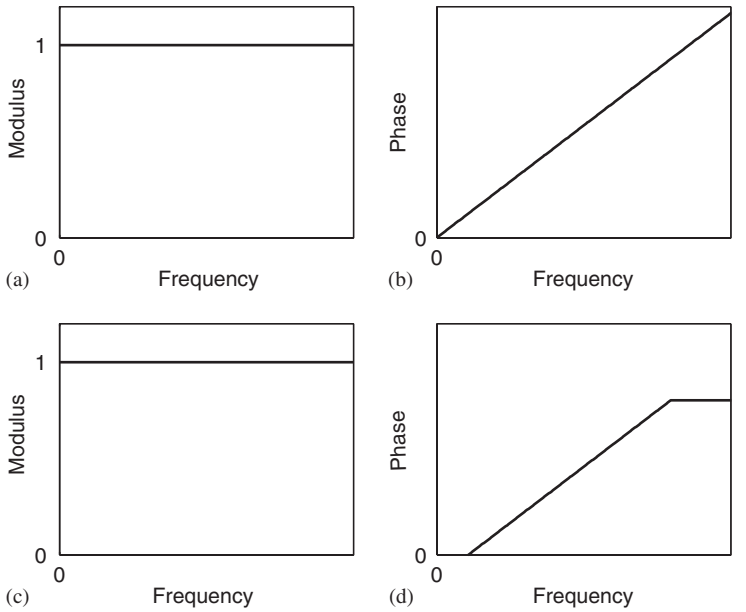

Fig. 5. The CSD of the PHAT estimator. In the ideal case (a) modulus; (b) phase. In the band-limited case (c) modulus; (d) phase.

Consider the simple case of the application of an ideal band-pass filter with frequency characteristics given by

$$G(\omega) = \begin{cases} 1, & \omega_0 \leqslant |\omega| < \omega_1, \\ 0, & \text{otherwise.} \end{cases} \tag{28}$$

The modified weighting function $\Psi_P(\omega)$ is then given by

$$\Psi_P(\omega) = \frac{G(\omega)}{|S_{x_1x_2}(\omega)|}. \tag{29}$$

Combined with Eq. (11), the PHAT estimator $R^P_{x_1x_2}(\tau)$ changes to

$$R^P_{x_1x_2}(\tau) = F^{-1}\{\Psi_P(\omega)S_{x_1x_2}(\omega)\} = g(\tau) \otimes \delta(\tau + T_0), \tag{30}$$

where

$$g(\tau) = F^{-1}\{G(\omega)\} = \frac{2\sin(\Delta\omega\tau/2)\cos(\omega_c\tau)}{\pi\tau},$$

and ω_c is the centre frequency $\omega_c = (\omega_0 + \omega_1)/2$. Eq. (30) can be reformulated as

$$R^P_{x_1x_2}(\tau) = \frac{2\sin[\Delta\omega(\tau + T_0)/2]\cos[\omega_c(\tau + T_0)]}{\pi(\tau + T_0)} \tag{31}$$

which shows that $R^P_{x_1x_2}(\tau)$ oscillates at the 'centre' frequency ω_c with modulation controlled by the bandwidth $\Delta\omega$. We define a temporal bandwidth $\Delta\tau$, which is also the resolution of the time delay estimate, as the time between the first two zero-crossings, given by

$$\Delta\tau = \frac{\pi}{\omega_c}. \tag{32}$$

This shows that the resolution of the time delay estimator can be improved by using a band-pass filter with a high centre frequency ω_c, which means, if possible, using a band-pass filter with a higher cut-off frequency ω_1. On the other hand, the oscillatory behaviour of the correlation function can be largely reduced by using a broad band-pass filter with a lower cut-off frequency ω_0 [15]. In practical situations, a distinct peak in the

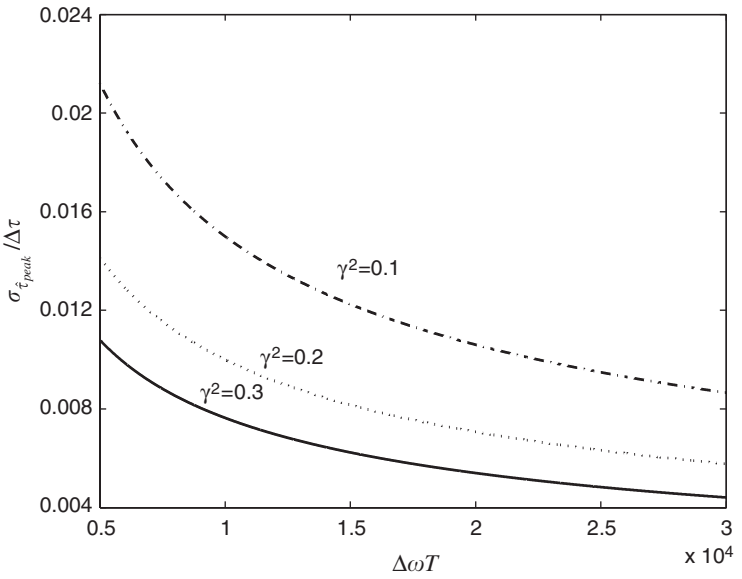

Fig. 6. The ratio of the standard deviation to the resolution for different values of coherence γ^2.

cross-correlation function is required to compensate for the effect of background noise. In this case, a broad band-pass filter is normally applied to suppress the spreading phenomenon of the cross-correlation function with the resolution of the time delay estimator given by Eq. (32). The lower frequency cut-off ω_0 is usually set to remove background noise and has a typical value of between 5 and 10 Hz in practice. As mentioned previously, the upper cut-off frequency ω_1 is normally governed by the pipe characteristics and the distances of the sensors from the leak.

The standard deviation and the resolution are of importance in influencing the accuracy of the time delay estimate. Combining Eq. (25) with Eq. (32) gives the ratio of $\sigma_{\hat{\tau}_{\text{peak}}}$ to $\Delta\tau$ as,

$$\frac{\sigma_{\hat{\tau}_{\text{peak}}}}{\Delta\tau} = \sqrt{\frac{3}{\pi}}\frac{1}{T^{1/2}}\frac{\sqrt{1-\gamma^2}}{\gamma}\frac{\omega_0 + \Delta\omega/2}{[(\omega_0+\Delta\omega)^3 - \omega_0^3]^{1/2}}. \tag{33}$$

If a broad band-pass filter is used, which satisfies the condition $\omega_0 \ll \Delta\omega$, Eq. (33) can be approximated by

$$\frac{\sigma_{\hat{\tau}_{\text{peak}}}}{\Delta\tau} \approx \frac{1}{2}\frac{\sqrt{1-\gamma^2}}{\gamma}\frac{1}{(\Delta\omega T)^{1/2}}. \tag{34}$$

Eq. (34) is plotted in Fig. 6. It can be seen that the ratio is much less than unity for all $\Delta\omega T$ and values of coherence γ^2. It decreases with increasing $\Delta\omega T$ and γ^2. This demonstrates that the random error (as estimated by the standard deviation) of the estimate due to the presence of noise on the measurements is generally insignificant compared to its resolution, which is only a function of the frequency bandwidth.

6. Comparison of time delay estimators applied to experimental data

The time delay estimators discussed in this paper were tested on experimental data measured at a specially constructed leak-detection facility located at a National Research Council site in Canada. The description of the test site and measurement procedures are detailed in Ref. [19]. A joint leak signal was measured using hydrophones and accelerometers. Referring to Fig. 1, the distance d between the two sensor signals was 102.6 m, and the distance d_1 from the leak to sensor 1 was 73.5 m. The signals were each passed through an anti-aliasing filter with the cut-off frequency set at 200 Hz. Hydrophone-measured signals of 66-s duration were then digitised at a sampling frequency of 500 samples/s. The same sampling frequency was applied to the accelerometer-measured signals for the time duration of 60 s.

Spectral analysis was performed on the digitised data using a 1024-point FFT, applying a Hanning window and averaging the power spectra. The modulus and phase of the CSD together with the coherence between the sensor signals are shown in Fig. 7 for both hydrophone and accelerometer-measured signals. Comparing

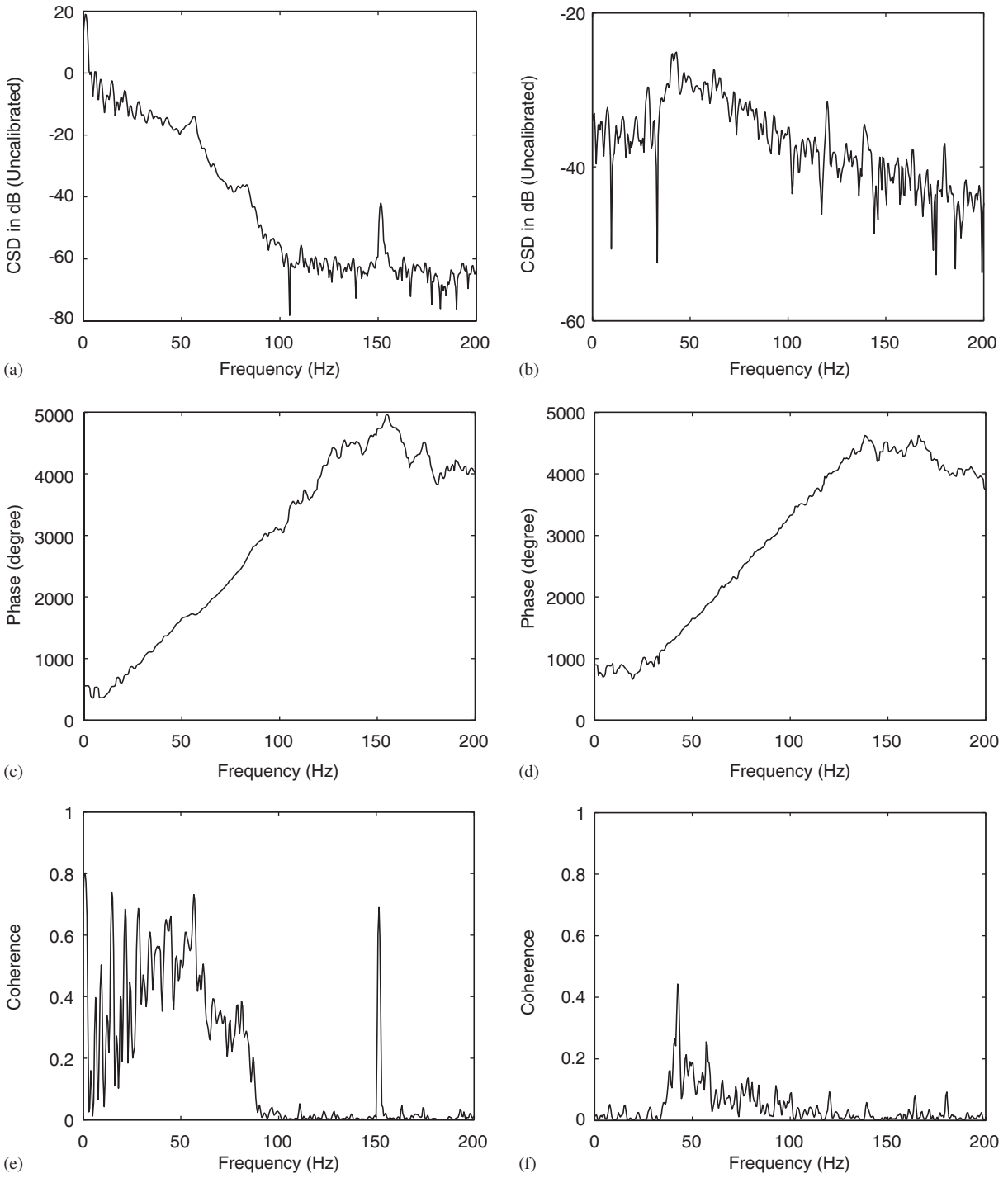

Fig. 7. Spectral analysis between two sensor signals. Hydrophone-measured signals: (a) modulus of the CSD; (c) phase spectrum; (e) coherence. Accelerometer-measured signals: (b) modulus of the CSD; (d) phase spectrum; and (f) coherence.

Figs. 7(a) and (b) it can be seen that the high-frequency pressure signals are attenuated significantly compared with the accelerometer signals. The reason for this is discussed in [18]. The phase spectra obtained from the sensor signals are shown in Figs. 7(c) and (d). Based on the gradients of the unwrapped phase spectra, the wavespeed is calculated as 479 and 484 m/s for hydrophone and accelerometer-measured signals, respectively. It can be seen from Figs. 7(e) and (f) that the coherence between the accelerometer-measured signals is much poorer than that for the hydrophone-measured signals.

The measured signals were then passed through a band-pass filter with cut-off frequencies set at 10 and 50 Hz for the hydrophone-measured signals, and 30 and 140 Hz for the accelerometer-measured signals.

The correlation functions obtained using the various estimators are plotted in Figs. 8 and 9 for hydrophone and accelerometer-measured signals, respectively. The results are normalised to the peak correlation values. In both cases, the pre-whitening process provided by the PHAT, SCOT and ML estimators, gives a more distinct peak correlation with a narrower peak and smaller variance, in comparison with other time delay estimators. For the cross-correlation functions of the hydrophone-measured signals shown in Fig. 8 the three GCC methods exhibit similar oscillatory behaviour. The explanation for this is the relatively high SNR for the

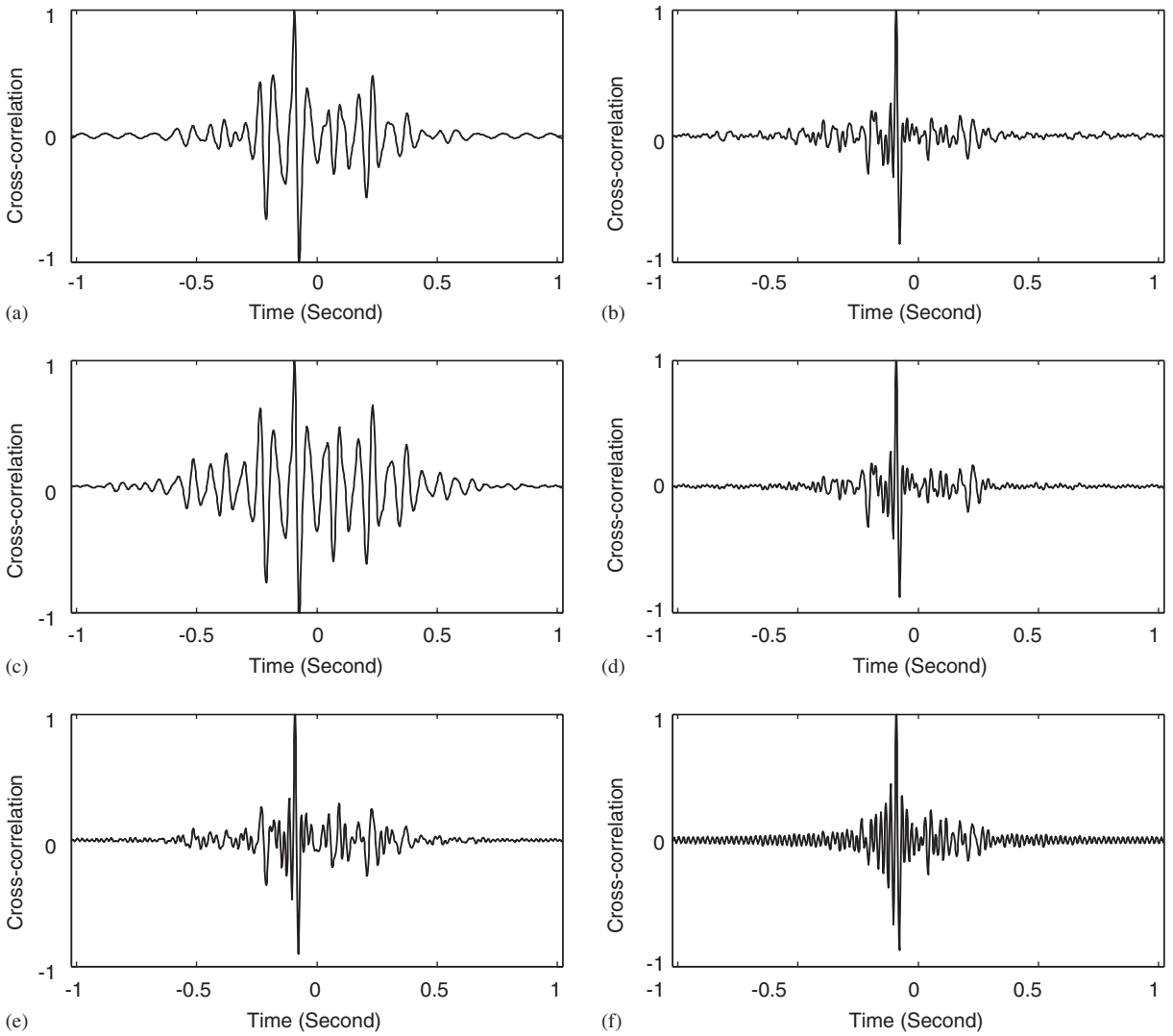

Fig. 8. Normalised cross-correlation using various correlation methods for hydrophone-measured signals: (a) BCC; (b) PHAT; (c) WIENER; (d) SCOT; (e) ML; (f) ROTH.

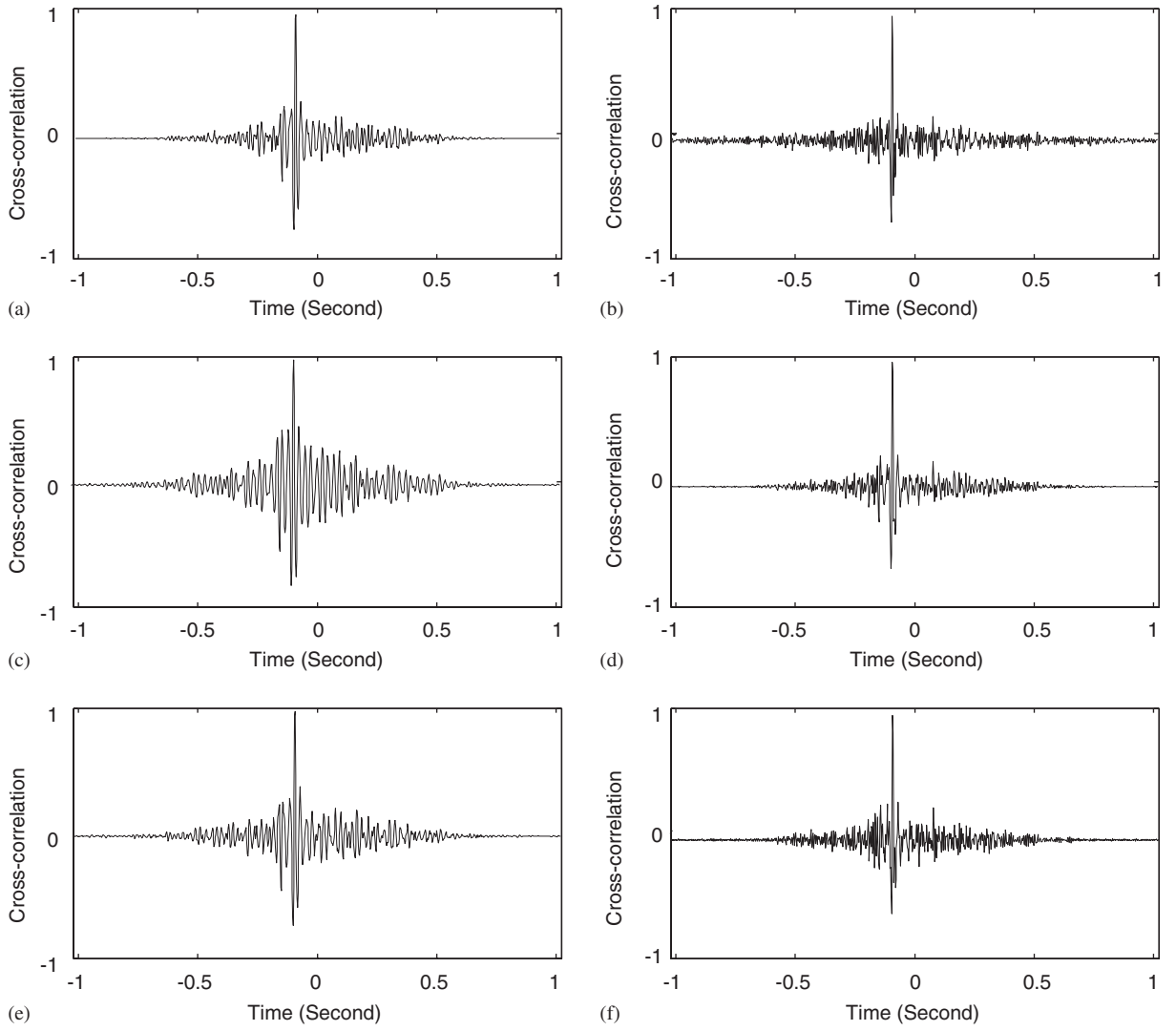

Fig. 9. Normalised cross-correlation using various correlation methods for accelerometer-measured signals: (a) BCC; (b) PHAT; (c) WIENER; (d) SCOT; (e) ML; (f) ROTH.

hydrophone measurements [18]. In the case of the low SNR present in the accelerometer measurements; however, large differences in the cross-correlation function can be seen, as shown in Fig. 9.

Figs. 8 and 9 show that, although the ML weighting leads to the minimum variance of the time delay estimate [9], the sharpest peak and lowest variance of the cross-correlation function are not necessarily achieved by using this estimator.

To evaluate the accuracy of the time delay estimates, the corresponding relative distance d_1 of the leak location was calculated and is shown in Table 2. Compared with the actual value $d_1 = 73.5$ m, the PHAT and SCOT estimators are the most accurate. The resolution imposed by band-pass filtering for the hydrophone-measured signals was 0.017 s, which causes 9% error in the distance d_1 (corresponding to a distance of 6.6 m). A broader band-pass filter is applied to the accelerometer-measured signals, which gives a resolution of $\Delta\tau = 0.006$ s and a corresponding error 3% in the distance d_1 (corresponding to a distance of 2.2 m).

The variance of the time delay estimators obtained by using the various cross-correlation methods can be determined from Eq. (22). As can be seen from Table 2, the ML estimator gives the minimum standard deviation of the time delay estimate for both hydrophone and accelerometer-measured signals. However, the

Table 2
Results of the time delay estimators and distance d_1

		BCC	PHAT	WIENER	SCOT	ML	ROTH
Hydrophone-measured data	$\hat{\tau}_{peak}$ (s)	−0.094	−0.092	−0.094	−0.092	−0.090	−0.090
	d_1 (m)	73.8	73.3	73.8	73.3	72.9	72.9
	$\sigma_{\hat{\tau}_{peak}}$ (e−4s)	1.128	0.764	1.011	0.695	0.652	0.742
Accelerometer-measured data	$\hat{\tau}_{peak}$ (s)	−0.090	−0.092	−0.090	−0.092	−0.090	−0.092
	d_1 (m)	73.1	73.6	73.1	73.6	73.1	73.6
	$\sigma_{\hat{\tau}_{peak}}$ (e−4s)	0.783	2.566	0.878	0.822	0.702	0.995

standard deviations of all the time delay estimators are small. The largest standard derivation is obtained for the PHAT estimator using accelerometer-measured signals, giving an error of 0.21 m, which is less than 0.3% of the distance calculated. In comparison with the resolution of the time delay estimate due to band-pass filtering, the standard deviations for all estimators are insignificant, and hence can be neglected in a practical procedure for leak detection in buried plastic water pipes.

7. Conclusions

In this paper, various time delay estimators have been compared for the purposes of leak detection in buried plastic water pipes. It has been shown that the PHAT, SCOT and ML estimators designed to pre-whiten the leak signals prior to the cross-correlation, have the desirable feature of sharpening the peak in the cross-correlation function. Although the PHAT estimator is designed to give a delta function located at the exact time delay, in practice the SCOT and ML estimators additionally take account of effect of background noise in the estimation procedure, which will probably be more beneficial to water leak detection. Moreover it has been found that the random error in the time delay estimates due to random noise on the measurements is generally insignificant compared to the resolution of the time delay estimate for leak detection in typical plastic pipes. Some limited experimental results confirm these findings.

Acknowledgements

The authors gratefully acknowledge the support of the EPSRC under grant GR/R13937/01 and test data provided by the National Research Council in Canada.

Appendix A. Variance of the time delay estimate

Despite the relatively widespread use of the expression for the variance of the time delay estimate derived by Carter [16], its derivation does not appear to exist elsewhere apart from his Ph.D. dissertation. This appendix derives the variance of the time delay estimate using the correlation technique, which is a similar approach to that taken by Carter. The derivation of the variance of the time delay estimate $\hat{\tau}_{peak}$ does not account for errors due to ambiguous peaks in the cross-correlation function and it is assumed that the estimated time delay is in the neighbourhood of the correct value.

The leak signals measured by acoustic/vibration sensors can be mathematically modelled by Eqs. (4) and (5). In the implementation of the GCC estimator $\hat{R}^g_{x_1x_2}(\tau)$ as illustrated in Fig. 3(a), the sensor signals $x_1(t)$ and $x_2(t)$ are filtered by $H_1(\omega)$ and $H_2(\omega)$, respectively. The frequency weighting function $\Psi_g(\omega)$ described in Section 3 is given by

$$\Psi_g(\omega) = H_1^*(\omega)H_2(\omega). \tag{A.1}$$

The variance of the time delay estimator $\sigma^2_{\hat{\tau}_{peak}}$ is the square of the standard deviation of the time delay estimator, $\sigma_{\hat{\tau}_{peak}}$, and is illustrated in Fig. A1(a). τ_{peak} is the abscissa value at which the GCC peaks and the

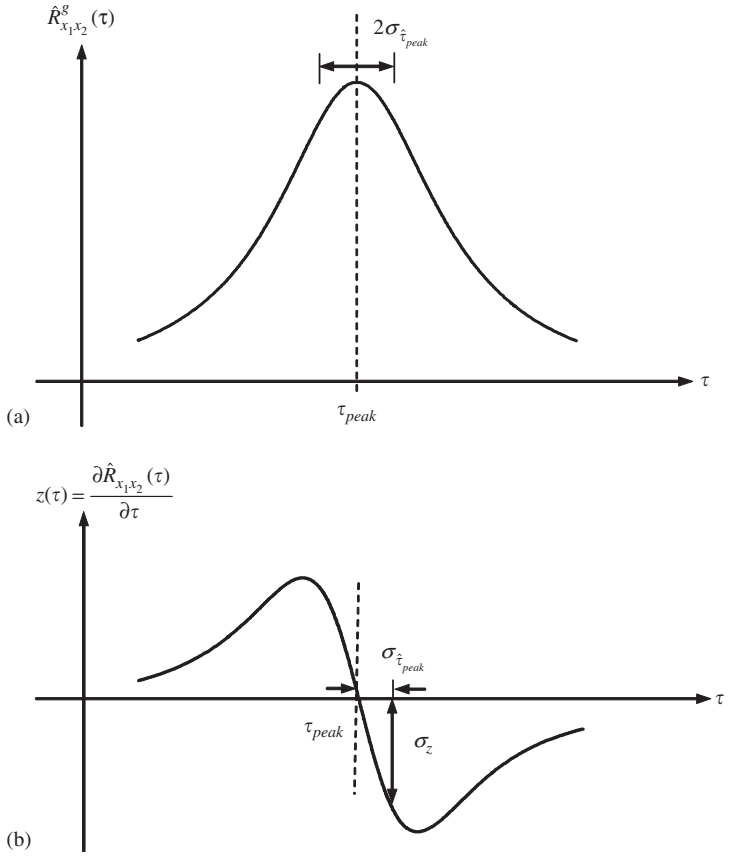

Fig. A1. Illustration of the determination of the variance of the time delay estimator. (a) Variance of the time delay estimator; and (b) the first derivative of the GCC function.

time delay estimator $\hat{\tau}_{\text{peak}}$ is located within the range $\tau_{\text{peak}} \pm \sigma_{\hat{\tau}_{\text{peak}}}$, where $\sigma_{\hat{\tau}_{\text{peak}}}$ denotes the standard deviation of $\hat{\tau}_{\text{peak}}$.

The corresponding first derivative of the GCC function with respect to the time τ, is given by

$$z(\tau) = \frac{\partial \hat{R}^g_{x_1x_2}(\tau)}{\partial \tau}, \tag{A.2}$$

and is plotted in Fig. A1(b). It can be seen from this figure that $\sigma_{\hat{\tau}_{\text{peak}}}$ is the left/right variation of the zero crossing of $z(\tau)$. The corresponding variation of z as shown in the figure is the standard deviation σ_z at $\tau = \tau_{\text{peak}}$. For small values of σ_z, the magnitude of the expected value of the slope of the output at $\tau = \tau_{\text{peak}}$ is given by

$$\left|\frac{\partial E[z]}{\partial \tau}\right|_{\tau=\tau_{\text{peak}}} = \left|\frac{\partial^2 E[\hat{R}^g_{x_1x_2}(\tau)]}{\partial \tau^2}\right|_{\tau=\tau_{\text{peak}}} = \left.\frac{\sigma_z}{\sigma_\tau}\right|_{\tau=\tau_{\text{peak}}}. \tag{A.3}$$

In order to solve Eq. (A.3) for $\sigma_{\hat{\tau}_{\text{peak}}} = \sigma_\tau|_{\tau=\tau_{\text{peak}}}$, $|\partial^2 E[\hat{R}^g_{x_1x_2}(\tau)]/\partial\tau^2|_{\tau=\tau_{\text{peak}}}$ and $\sigma_z|_{\tau=\tau_{\text{peak}}}$ must be known. In practice, only an estimate $\hat{S}_{x_1x_2}(\omega)$ of the cross-spectral density (CSD) can be obtained from the finite observations of $x_1(t)$ and $x_2(t)$. For large observation time $T \to \infty$, the expectation of $\hat{S}_{x_1x_2}(\omega)$ is

$$E[\hat{S}_{x_1x_2}(\omega)] = S_{x_1x_2}(\omega) = |S_{x_1x_2}(\omega)|e^{-i\omega\tau_{\text{peak}}}. \tag{A.4}$$

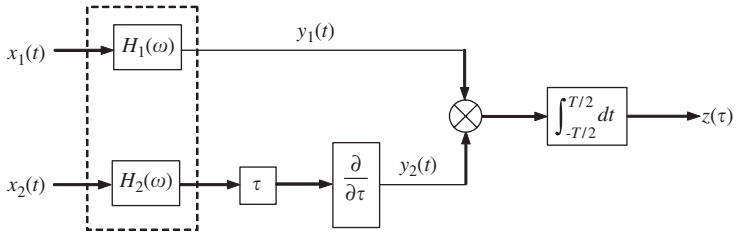

Fig. A2. Process to determine the first derivative of the GCC, $z(\tau)$.

Combining Eq. (A.4) with Eq. (11) gives

$$\left|\frac{\partial^2 E[\hat{R}^g_{x_1x_2}(\tau)]}{\partial\tau^2}\right|_{\tau=\tau_{\text{peak}}} = \frac{1}{2\pi}\int_{-\infty}^{+\infty} \omega^2 \Psi_g(\omega)|S_{x_1x_2}(\omega)|\,\mathrm{d}\omega. \tag{A.5}$$

Thus one term in Eq. (A.3) can be determined in a straightforward manner. It remains to find $\sigma_z|_{\tau=\tau_{\text{peak}}}$ and this requires some straightforward but tedious algebra and is described next. Based on the commutativity of integration and differentiation, Fig. A2 shows the process to determine the first derivative of the GCC function $z(\tau)$, which can be obtained from

$$z(\tau) = \frac{1}{T}\int_{-T/2}^{T/2} y_1(t)y_2(t)\,\mathrm{d}t, \tag{A.6}$$

where $y_1(t)$ is assumed to be the output of the filter $H_1(\omega)$ excited by signal $x_1(t)$, and $y_2(t)$ is the output of a filter $H_2(\omega)$ excited by signal $x_2(t)$ cascaded with a time delay τ and a differentiator, as shown in Fig. A2.

In the frequency domain, the corresponding auto and cross-spectral densities of $y_1(t)$ and $y_2(t)$ satisfy the relations given by

$$S_{y_1y_1}(\omega) = |H_1(\omega)|^2 S_{x_1x_1}(\omega), \tag{A.7}$$

$$S_{y_2y_2}(\omega) = \omega^2|H_2(\omega)|^2 S_{x_2x_2}(\omega), \tag{A.8}$$

$$S_{y_1y_2}(\omega) = \mathrm{i}\omega \mathrm{e}^{\mathrm{i}\omega\tau} H_1^*(\omega)H_2(\omega)S_{x_1x_2}(\omega). \tag{A.9}$$

By definition, the variance of the first derivative of the GCC function is given by

$$\sigma_z^2 = E[z^2] - E^2[z], \tag{A.10}$$

where

$$\begin{aligned} E[z] &= \lim_{T\to\infty} E\left[\frac{1}{T}\int_{-T/2}^{T/2} y_1(t)y_2(t)\,\mathrm{d}t\right] \\ &= \lim_{T\to\infty}\frac{1}{T}\int_{-T/2}^{T/2} E[y_1(t)y_2(t)]\,\mathrm{d}t \\ &= R_{y_1y_2}(0); \end{aligned} \tag{A.11}$$

and

$$E[z^2] = \lim_{T\to\infty}\frac{1}{T^2}\int_{-T/2}^{T/2}\int_{-T/2}^{T/2} E[y_1(t_1)y_2(t_1)y_1(t_2)y_2(t_2)]\,\mathrm{d}t_1\,\mathrm{d}t_2. \tag{A.12}$$

The fourth moment in Eq. (A.12) can be derived by assuming that $y_1(t)$ and $y_2(t)$ are jointly stationary Gaussian processes. Eq. (A.12) then becomes [16]

$$E[z^2] = \lim_{T\to\infty}\frac{1}{T^2}\int_{-T/2}^{T/2}\int_{-T/2}^{T/2}[R_{y_1y_2}^2(0) + R_{y_1y_1}(t_2-t_1)R_{y_2y_2}(t_2-t_1) + R_{y_1y_2}(t_2-t_1)R_{y_2y_1}(t_2-t_1)]\,\mathrm{d}t_1\,\mathrm{d}t_2. \tag{A.13}$$

Substituting Eqs. (A.11) and (A.13) into Eq. (A.10) and letting $t_0 = t_2 - t_1$ gives

$$\sigma_z^2 = \lim_{T\to\infty}\frac{1}{T^2}\int_{-T/2}^{T/2}\int_{-T/2}^{T/2}[R_{y_1y_1}(\tau)R_{y_2y_2}(\tau) + R_{y_1y_2}(\tau)R_{y_2y_1}(\tau)]\,\mathrm{d}t_0\,\mathrm{d}t_1. \tag{A.14}$$

Integrating Eq. (A.14) with respect to t_1 gives

$$\sigma_z^2 = \lim_{T\to\infty}\frac{1}{T}\int_{-T/2}^{T/2}[R_{y_1y_1}(t_0)R_{y_2y_2}(t_0) + R_{y_1y_2}(t_0)R_{y_2y_1}(t_0)]\,\mathrm{d}t_0. \tag{A.15}$$

Making use of the Parseval's Theorem (Power Theorem), Eq. (A.15) can be rewritten as

$$\sigma_z^2 = \frac{1}{2\pi T}\int_{-\infty}^{\infty}[S_{y_1y_1}(\omega)S_{y_2y_2}(\omega) + S_{y_1y_2}^2(\omega)]\,\mathrm{d}\omega. \tag{A.16}$$

Substituting Eqs. (A.7)–(A.9) into Eq. (A.16) gives

$$\sigma_z^2 = \frac{1}{2\pi T}\int_{-\infty}^{\infty}\omega^2|\Psi_g(\omega)|^2 S_{x_1x_1}(\omega)S_{x_2x_2}(\omega)\left[1 - \mathrm{e}^{2\mathrm{i}\omega\tau}\frac{S_{x_1x_2}^2(\omega)}{S_{x_1x_1}(\omega)S_{x_2x_2}(\omega)}\right]\mathrm{d}\omega. \tag{A.17}$$

Noting that $S_{x_1x_2}(\omega)$ is determined by Eq. (A.4), Eq. (A.17) can be rewritten as

$$\sigma_z^2 = \frac{1}{2\pi T}\int_{-\infty}^{\infty}\omega^2|\Psi_g(\omega)|^2 S_{x_1x_1}(\omega)S_{x_2x_2}(\omega)\left[1 - \mathrm{e}^{2\mathrm{i}\omega\tau}\mathrm{e}^{-2\mathrm{i}\omega\tau_{\mathrm{peak}}}\frac{|S_{x_1x_2}(\omega)|^2}{S_{x_1x_1}(\omega)S_{x_2x_2}(\omega)}\right]\mathrm{d}\omega. \tag{A.18}$$

When $\tau = \tau_{\mathrm{peak}}$, Eq. (A.18) reduces to

$$\sigma_z^2\big|_{\tau=\tau_{\mathrm{peak}}} = \frac{1}{2\pi T}\int_{-\infty}^{\infty}\omega^2|\Psi_g(\omega)|^2 S_{x_1x_1}(\omega)S_{x_2x_2}(\omega)[1-\gamma_{x_1x_2}^2(\omega)]\,\mathrm{d}\omega. \tag{A.19}$$

Finally Eqs. (A.5) and (A.19) can be substituted into Eq. (A.3) to yield

$$\sigma_{\hat{\tau}_{\mathrm{peak}}}^2 = \frac{2\pi}{T}\frac{\int_{-\infty}^{\infty}\omega^2|\Psi_g(\omega)|^2 S_{x_1x_1}(\omega)S_{x_2x_2}(\omega)[1-\gamma_{x_1x_2}^2(\omega)]\,\mathrm{d}\omega}{\left[\int_{-\infty}^{\infty}\omega^2\Psi_g(\omega)|S_{x_1x_2}(\omega)|\,\mathrm{d}\omega\right]^2}, \tag{A.20}$$

which gives the variance of the time delay estimate and is the same as that reported by Carter in Ref. [16].

References

[1] M. Fantozzi, G.D. Chirico, E. Fontana, F. Tonolini, Leak inspection on water pipelines by acoustic emission with cross-correlation method, in: *Annual Conference Proceeding, American Water Works Association, Engineering and Operations*, San Antonio, 1993, pp. 609–721.

[2] H.V. Fuchs, R. Riehle, Ten years of experience with leak detection by acoustic signal analysis, *Applied Acoustics* 33 (1991) 1–19.

[3] D.A. Liston, J.D. Liston, Leak detection techniques, *Journal of the New England Water Works Association* 106 (1992) 103–108.

[4] J.M. Muggleton, M.J. Brennan, R.J. Pinnington, Wavenumber prediction of waves in buried pipes for water leak detection, *Journal of Sound and Vibration* 249 (5) (2002) 934–954.

[5] J.M. Muggleton, M.J. Brennan, P.W. Linford, Axisymmetric wave propagation in fluid-filled pipes: wavenumber measurements in in vacuo and buried pipes, *Journal of Sound and Vibration* 270 (1–2) (2003) 171–190.

[6] O. Hunaidi, W. Chu, Acoustical characteristics of leak signals in plastic water distribution pipes, *Applied Acoustics* 58 (3) (1999) 235–254.

[7] C.H. Knapp, G.C. Carter, The generalised correlation method for estimation of time delay, *IEEE Transactions on Acoustics, Speech, and Signal Processing* 24 (4) (1976) 320–327.

[8] J.C. Hassab, R.E. Boucher, Optimum estimation of time delay by a generalised correlator, *IEEE Transactions on Acoustics, Speech, and Signal Processing* 27 (4) (1979) 373–380.
[9] G.C. Carter, Coherence and time delay estimation, *Proceedings of the IEEE* 75 (2) (1987) 236–255.
[10] P.R. Roth, Effective measurements using digital signal analysis, *IEEE Spectrum* 8 (1971) 62–70.
[11] G.C. Carter, A.H. Nuttall, P.G. Cable, The smoothed coherence transform, *Proceedings of the IEEE* 61 (1973) 1497–1498.
[12] G.C. Carter, A.H. Nuttall, P.G. Cable, The smoothed coherence transform (SCOT). Naval Underwater Systems Centre: New London, CT, *Tech. Memo* TC-159-72, 1972.
[13] E.J. Hannan, P.J. Thomson, Estimating group delay, *Biometrika* 60 (1973) 241–253.
[14] A.O. Hero, S.C. Schwartz, A new generalised cross correlator, *IEEE Transactions on Acoustics, Speech, and Signal Processing* 33 (1) (1985) 38–45.
[15] Y. Gao, M.J. Brennan, P.F. Joseph, J.M. Muggleton, O. Hunaidi, A model of the correlation function of leak noise in buried plastic pipes, *Journal of Sound and Vibration* 277 (1–2) (2004) 133–148.
[16] G. C. Carter, Ph.D. Dissertation: Time delay estimation. Univ. Connecticut, 1976.
[17] A.V. Oppenheim, R.W. Schafer, *Digital Signal Processing*, Prentice-Hall, Englewood Cliffs, NJ, 1975.
[18] Y. Gao, M.J. Brennan, P.F. Joseph, J.M. Muggleton, O. Hunaidi, On the selection of acoustic/vibration sensors for leak detection in plastic water pipes, *Journal of Sound and Vibration* 283 (3–5) (2005) 927–941.
[19] O. Hunaidi, W. Chu, A. Wang, W. Guan, Detecting leaks in plastic pipes, *Journal of American Water Works Association* 92 (2) (2000) 82–94.